Article

Synthesis and Characterization Iron Oxide Nanoparticles (α-Fe_2O_3 NPs) For Removal of Eriochrome Black T Form Aqueous Solution: Expermantal and DFT Study

Noor Ali Einad, Mudeer Mubarak Merza and Ahmad Hussian Ismail

Department of Chemistry, College of Science, Mustansiriyah University, Baghdad, Iraq

Corresponding author: noor1995ali19951@gmail.com

Abstract

The aim of this work is to explore the elimination of Eriochrome Black T from a water solution using iron oxide nanoparticle adsorbent. α-Fe_2O_3 NPs were produced using the green process and characterized using a variety of methods, including EDX, XRD, and SEM. Batch adsorption tests were conducted with a number of variables, including contact duration, effect PH, and temperature. The results revealed that Eriochrome Black T had the maximum removal efficacy on α-Fe_2O_3 NPs after 150 minutes of contact. The equilibrium data were well suited to the Freundlich model. Kinetic studies show that the pseudo-second-order model may represent Eriochrome Black T methods of adsorption. the thermodynamic investigation indicate the adsorption process is a exothermic and spontaneous in nature.

We performed DFT calculations using Gaussian 09 with B3LYP/6-311G(d,2p) basis sets to study the interaction between Eriochrome Black T dye (EBT) and α-Fe_2O_3 NPs. The results indicate significant shifts in highest occupied molecular orbital (HOMO), and the lowest unoccupied molecular orbital (LUMO) energies and an increased energy gap, suggesting chemisorption and decreased stability of the EBT-Fe_2O_3 NPs complex compared to isolated α-Fe_2O_3 NPs.

Keywords: Adsorption, DFT study, Eriochrome Black T dye, Green method, α-Fe_2O_3 NPs, Nanomaterials.

1. Introduction

Pollution considered as a major problem that threatens the environment which has harmful effects on animals, plants, and human beings [1,2]. It causes poison of the soil and water sources

and the erosion of the gaseous atmosphere through increasing different anthropogenic activities such as incessant combustion of fossil fuels, which release gaseous pollutants, disposal of organic waste into water streams, destroying aquatic life, forest destruction and causing poor and polluted air quality, damaging the soil fertility via plastic waste littering [3]. Water pollution due to industrial and human activities is the main cause that leads to 80% of diseases worldwide. According to United Nations reports, there are about 1.1 billion people who do not have access to safe drinking water, and most of them are from poor and developing countries [4,5]. Major water contaminants are categorized into pathogens, inorganic and organic chemicals which include heavy metals, dyes, plastics, oil, pesticides, and volatile organic compounds (VOC) [6,7]. Dyes are Complicated unsaturated organic materials that can absorb light and give clear colors to the visible region [8]. In addition, it is a substance chromophore distinguished with absorbing spectrum parts of the visible region [9]. Eriochrome black T (EBT) is a commonly found dye in wastewater, a reactive and acidic dye with a conjugated azo (-N=N-) group as a chromophore [10,11]. EBT can be harmful to human health and the environment, while also harming aquatic organisms [12,13].

Nanomaterials are an intriguing class of materials that includes a wide variety of samples with at least one dimension between 1 and 100 nm [14,15]. Nanomaterials also have many excellent physicochemical properties, including, large surface area, small size, high chemical reactivity, cost-effectiveness and strong adsorption capacity [16,17]. Among nanomaterial is iron oxide nanoparticle, The three primary types of Iron oxide FeO, Fe_2O_3, and Fe_3O_4 [18,19]. On other hand, α-Fe_2O_3 NPs (hematite) is an important categories of Iron oxide that has unique size and shape-dependent characteristics and a wide variety of potential applications [20,21]. Among these applications is the field of purifying polluted water, which has promising prospects as an adsorbent for clean-up α-Fe_2O_3 NPs have high surface areas, many active sites, and a high capacity for adsorption of dyes and heavy metals [22] Various types of iron oxide nanoparticles have been synthesized using extracts from plants and their parts [23]. Plant extracts commonly contain terpenoids, sugars, alkaloids, polyphenols, proteins, and phenolic acids [24], which are responsible for the reducing and stabilization of metal oxide nanoparticles [25].

The aim of this study is to synthesize iron oxide nanoparticles (α-Fe_2O_3 NPs) by the green method and use them as adsorbents to remove Eriochrome Black T dye from an aqueous solution.

2. Experimental part

2.1. Materials

Ocimum basilicum plant. Anhydrous iron nitrate (Sigma Aldrich supplied analytical grade purity 95%). De-ionized water.

2.2 Preparation of plant extract

The collected leaves were washed with tap water to eliminate dust particles. To eliminate moisture, the leaves were washed with deionized water and shade-dried for 7 days. The dried leaves were pulverized in a grinder mixer and stored in the dark at room temperature. To create the plant extract, combine 5 g of dried leaf powder with 50 mL of deionized water in a 100-mL flask. Mix thoroughly on a magnetic stirrer with a heated plate at 60 °C for 10 minutes. The resulting extract was filtered. The filtrate was used immediately or stored at 4°C for future use.

2.2.1. Synthesis of iron oxide nanoparticles (α-Fe_2O_3 NPs)

0.02 molar of aqueous iron nitrate $Fe(NO_3)_2$, was synthesized by dissolving 5 g of it in 50 mL of non-ionic water and adding 5 g of plant extract by dissolving 5 g of it in 50 mL of non-ionic water with sonication for 10 minutes using the ultrasonic device. After that, 20 mL of 1N NaOH solution was added to the solution. After that, the solution was sonicated for 15 minutes using the ultrasonic. A brown precipitate appeared due to iron hydroxide $Fe(OH)_2$. It was separated using centrifugation and washed multiple times with deionized water. Thereafter, the precipitate was dried at 90 °C for about three hours. Then it was calcined at 480 °C for 3 hours.

2.3. Experimental adsorption

Adsorption tests were performed using Eriochrome Black T ($C_{20}H_{12}N_3O_7SNa$) at various concentrations (5, 10, 15, 20, and 25 ppm). The adsorbent was added in various quantities (0.01, 0.05, 0.1, 0.15and 0.2 g) add 10 ml of a mixture including a specific concentration of Eriochrome Black T. The volumetric container and its contents were then placed in a shaker vacuum and swirled continuously at 120 rpm. With period time in the range of 10–160 minutes, equilibrium time was achieved at 90 minutes. The mixture was then centrifuged for 15 min for separation (α-Fe_2O_3 NPs). Following adsorption, the dye solution's absorbance was UV/vis spectroscopy was

performed at an effective wavelength of 539 nm. The amount of adsorbate and removal efficiency were calculated according to the following equation [26,27]:

$$Qe = \frac{(C_0 - Ce)V}{M} \quad \text{.....(1)}$$

$$R\% = \frac{(C_0 - Ce)}{C_0} \times 100\% \quad \text{.....(2)}$$

where C_0 is concentration of Eriochrome Black T at initial time, Ce is concentration of Eriochrome black at equilibrium time, V is the volume of dye solution (L), and M is mass of nanomaterial.

3. Results and discussion

3.1. Characterization

3.1.1. The SEM image and EDX spectra for the Fe O_3-NPs are shown in Figure 1. SEM images of α-Fe_2O_3 NPs revealed Plate-like structure formation was observed in α-Fe_2O_3 NPs with agglomeration form. The agglomeration of NPs that appeared in the SEM images was likely due to magnetic nature of these particles [28].

In the EDX spectra (Figure1-b), the peaks around 0.8, 6.2, and 6.9 keV are related to the binding energies of Fe. Therefore, the EDX spectra for the Fe_2O_3/plant extract confirmed the presence of Fe_2O_3-NPs in the BS aqueous extract without any impurity peaks.

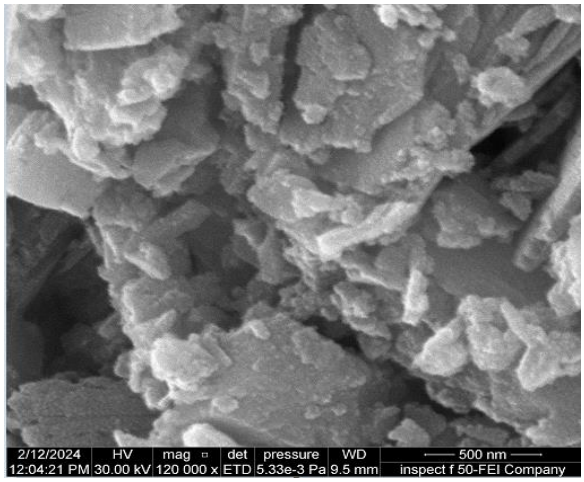

Figure (1-a): SEM image of α-Fe_2O_3 NPs

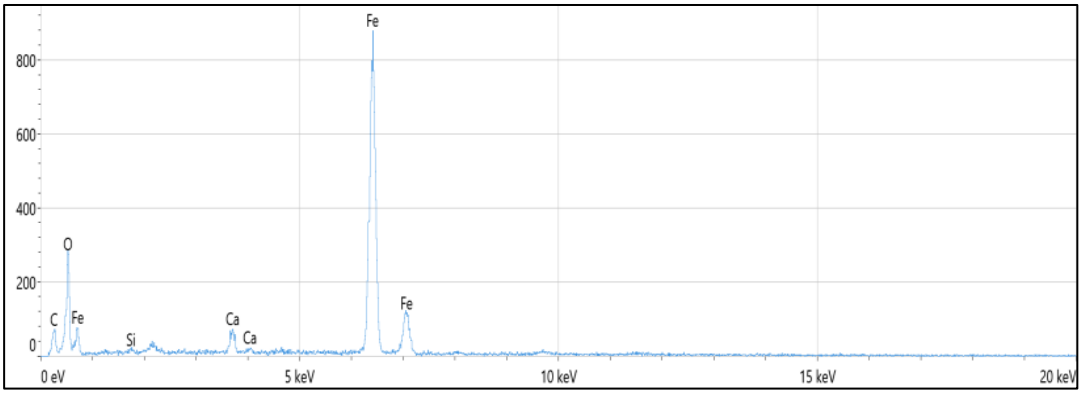

Figure (1-b): EDX image of α-Fe_2O_3 NPs

3.1.2. The α-Fe_2O_3 NPs diffraction peaks were centered at 2θ = 24.2˚, 33.49°, 35.67°, 40.94˚, 49.57°, 54.2°, 62.2◦, and 63.0◦ The diffraction peaks correspond to (012), (104), (110), (113), (024), (116), (0 1 8), and (2 1 4), respectively. All the reported diffractions are perfectly indexed with JCPDS card 33-0664, implying a single-phased α-Fe_2O_3 NP with a rhombohedral crystal structure [29]. The average size of α-Fe_2O_3 NPs was found to be 35.96.

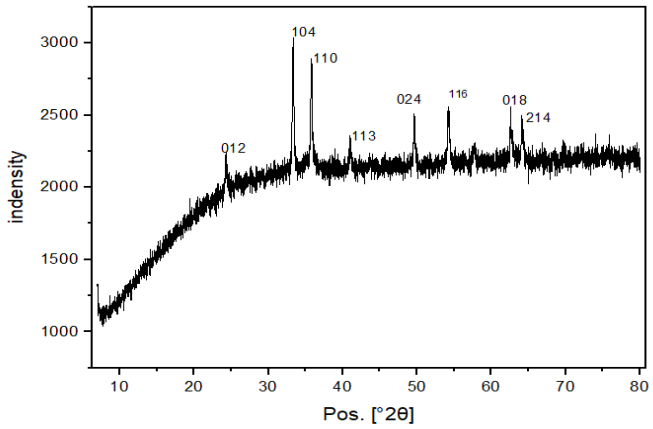

Figure 2: XRD of α-Fe_2O_3 NPs

3.2. Adsorption study

3.2.1. Effect of the contact time

The effect of contact time was studies by added 0.01 g of (α-Fe_2O_3 NPs) to 10mL Eriochrome Black T Solution (50ppm) at 25°C with a stirring speed of 120 rpm in various intervals of time (10-160) minutes. Fig.5 shows the effect of connect time in adsorption of, it is observed that

the removal efficiency increases directly with the increase the contact time, reached equilibrium within 150 min. after that, the rate of the adsorption process became constant, in order to saturate the active sites with adsorbate molecules [30].

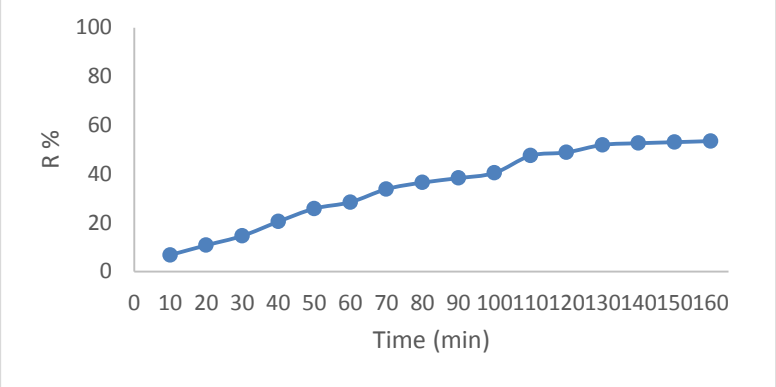

Figure 3: Effect time of adsorption of EBT onto α-Fe_2O_3 NPs

3.2.2 Effect of PH

One of the most essential characteristics explored was the acidity function (pH), along with the fixation of other parameters [31]. This study was carried out in different acidity function (PH 1, 3, 5, 7, 10, and 12), but the rest of the variables remained constant. The results revealed that the Eriochrome Black-T dye was removed more in the acidic environment than in the neutral and basic environments, which is attributable to the presence of extra H+ ions competing with the dye's anionic groups for adsorption sites. However, adsorption of dye decreases in the basic environment due to the anionic groups in the dye cause electrostatic repulsion between OH- groups. This describes the ion exchange mode of adsorption [32].

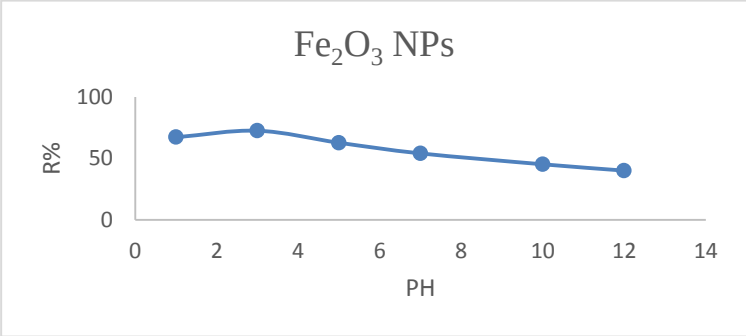

Figure 4: Effect PH of adsorption of EBT onto α-Fe_2O_3 NPs

2.2.3 Effect of the dosage of adsorbent

The effect of the dosage of α-Fe_2O_3 NPs on the removal efficiency of EBT was studied, as shown in figure (5). Through this study it was found the adsorption decrease with increase of adsorbent mass, the greater the agglomeration due to the decrease in surface area and thus the decrease in the number of active sites on the surface of the adsorbent, this can be attributed to the magnetic nature of iron oxide particles.

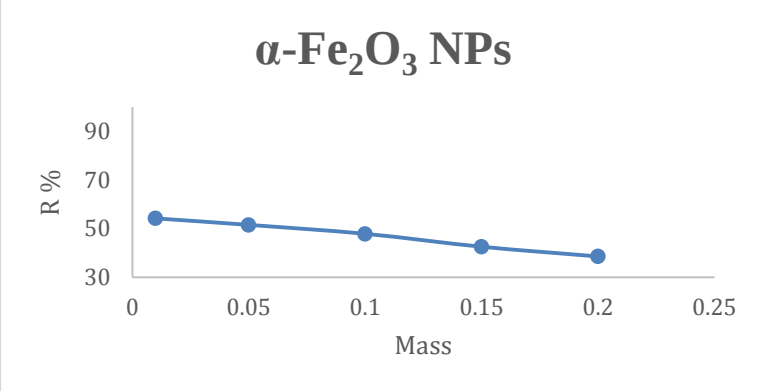

Figure 5: Effect mass of adsorption of EBT onto α-Fe_2O_3 NPs

3.2.4 The effect of Temperature and thermodynamic parameter

At a given temperature range of 288 to 328, the effect of temperature on the adsorption of Eriochrome Black T onto Fe_2O_3 adsorbent was investigated. When the temperature increased from 288 to 328 K, that indicate that the Eriochrome Black T may move from the solution phase to the adsorbent surface due to greater adsorption at greater temperatures due to the increased kinetic energy of dye molecules.

The thermodynamic parameters reveal specific information about the mechanism and nature of the adsorption process [33]. The thermodynamic parameters were determine using the following equations [34,35]:

$$ln\ ln\ (Ke) = \frac{-\Delta H}{RT} + \frac{\Delta S}{R} \quad \ldots\ldots\ldots\ldots\ldots\ldots (3)$$

$$Ke = \frac{Qe}{Ce} \ldots\ldots\ldots\ldots\ldots\ldots (4)$$

$$\Delta G = \Delta H - T\Delta S \ldots\ldots\ldots\ldots\ldots\ldots (5)$$

where Ke is an equilibrium constant, R is a gas constant (8.314 J/mole.K), and T is the temperature (K)

As shown in Table 1, the values of ΔG and ΔH is negative at all temperatures, suggest that the adsorption process is exothermic and spontaneous in nature [36]. And the values of ΔS is positive indicating that the more randomness of the system [37].

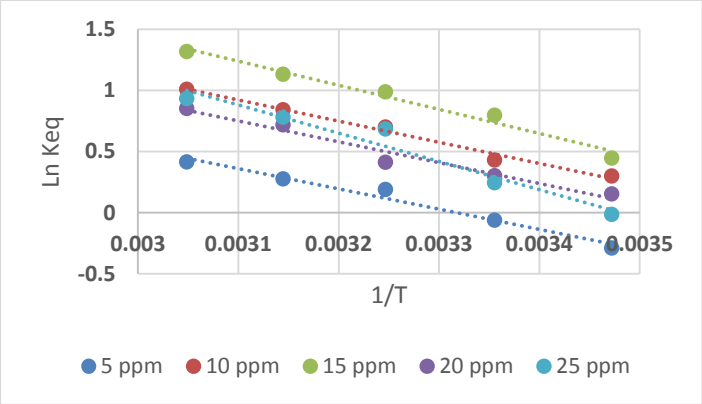

Figure 6: Van't Hoff plots of EBT adsorption onto (α-Fe_2O_3 NPs) at different temperature.

Table (1). Thermodynamic parameters for the adsorption of EBT onto (α-Fe_2O_3 NPs)

ΔH (kJ/mole)	ΔS (J\mole)	ΔG				
		288	298	308	318	328
-13.78	45.711	-26.94	-27.4	-27.86	-28.31	-28.77
-14.38	52.253	-29.43	-29.95	-30.48	-31	-31.52
-16.37	61.051	-33.95	-34.57	-35.18	-35.79	-36.4
-14.19	50.207	-28.65	-29.15	-29.65	-30.15	-30.65
-19.23	66.935	-38.51	-39.18	-39.84	-40.51	-41.18

3.2.5 Adsorption Kinetics

Kinetic study of adsorption process is necessary to obtain effective and useful information about the adsorption mechanism, that depends on the chemical and physical characteristics [38] [39]. The experimental data was described by pseudo-first-order model (PFOM) and pseudo-second-order (PSOM) model. The formulae pseudo-first-order equation [40]:

$\ln(qe - qt) = \ln(qe) - k1t$ …..(6)

The pseudo-second-order equation [41]:

$$\frac{1}{qt} = \frac{1}{k2qe} + \frac{t}{qe} \ldots\ldots (7)$$

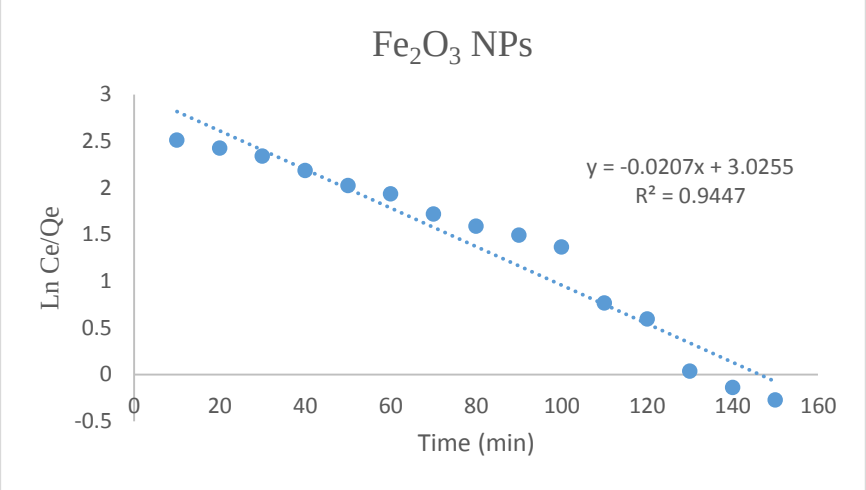

Figure 7: PFOM plots for the adsorption of EBT onto α-Fe_2O_3 NPs at 298 K

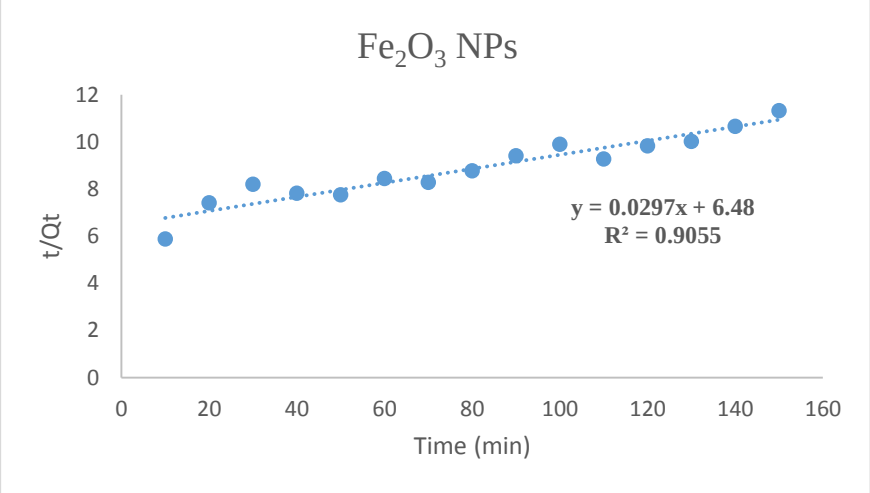

Figure 8: PSOM plots for the adsorption of EBT onto α-Fe_2O_3 NPs at 298 K

The kinetic information may be accurately described by a pseudo-first-order model with a high correlation coefficient ($R^2 > 0.9447$) of α-Fe_2O_3 NPs. The assumption is that the adsorption rate is controlled by the diffusion of dye molecules on the surface of α-Fe_2O_3 NPs [42].

3.2.6 Adsorption Isotherms

Adsorption isotherms provide crucial details adsorption capacity and properties of the surface of adsorbent which aid in understanding the interaction between the adsorbate and adsorbent [43,44]. In this study, The Freundlich and Langmuir isotherm models were then used to evaluate the adsorption of Eriochrome Black T onto (α-Fe_2O_3 NPs). These models are represented by Equations (8) and (9), respectively [45] [46]:

$$\frac{Ce}{qe} = \frac{1}{(qmax)\,Kl} + \frac{Ce}{qmax} \quad \ldots\ldots\ldots\ldots\ldots(8)$$

$$log\ log\ (Qe) = log\ log\ (kf) + \frac{1}{n}\ lo(Ce) \quad \ldots\ldots\ldots(9)$$

In these equations, k_F represents the Freundlich constant, n is a Adsorption intensity. q_{max} (mg/g) represents the theoretical maximal absorption capacity of dye, k_L (L/mg) represents the Langmuir constant.

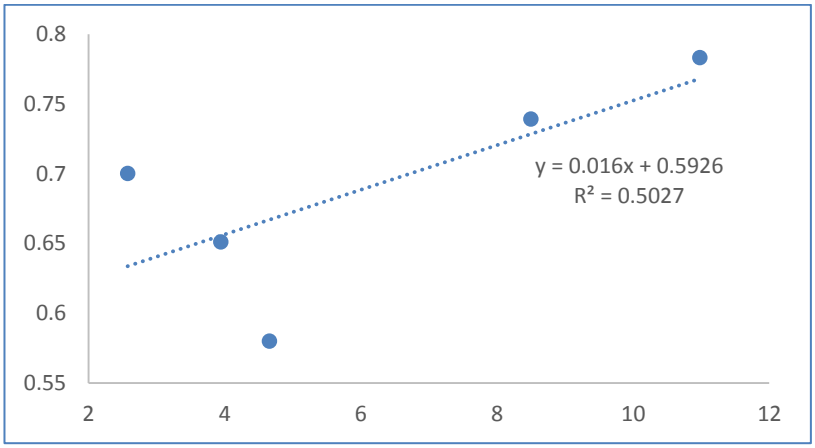

Figure 9: Langmuir isotherm for adsorption of EBT onto α-Fe_2O_3 NPs

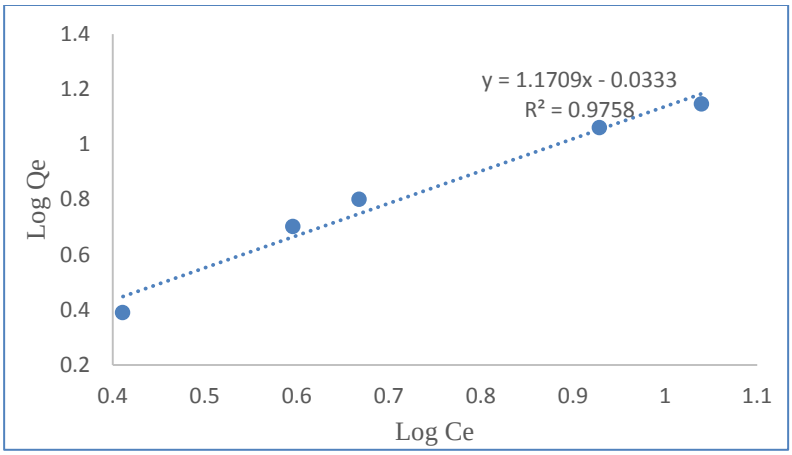

Figure 10: Freundlich isotherm for adsorption of EBT onto α-Fe_2O_3 NPs

According to the correlation coefficient (R^2) values, the Freundlich isotherm models closely suit to the equilibrium data, which suggested the multilayer adsorption [47].

Table (2): valuate constant Langmuir and Freundlich for the adsorption of EBT

Langmuir		Freundlich	
KL	-0.01715	Kf	0.6627
RL	1.750547	N	0.673
R^2	0.5027	R^2	0.9598

3.3 DFT calculations

To get theoretical insights that could support and enhance experimental results, we performed DFT calculations on the interaction of the molecule, Eriochrome black T dye (EBT), and Fe_2O_3 NPs. The compound was built using the ChemDraw of Mopac program, and the equilibrium geometries were found using the Gaussian 09 package. The geometry of the studied molecule in the vacuum medium was calculated using density functional theory (DFT) with the (B3LYP) and 6-311G (d, 2p) basis sets [48,49]. Figure 11 depicts the equilibrium EBT geometry after applying the most precise approaches (DFT (B3LYP/6-311G (d,2p)).

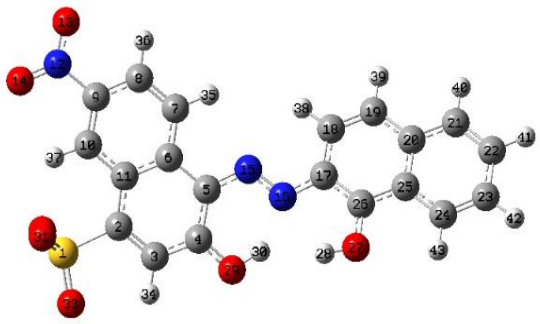

Figure 11: The equilibrium EBT geometry

The energies of the border molecular orbitals, the highest occupied molecular orbital (HOMO), and the lowest unoccupied molecular orbital (LUMO) are significant electronic characteristics to evaluate the reactivity and stability of the EBT-Fe_2O_3. Table (3) lists the HOMO and LUMO energies, as well as their gaps (in eV), for Eriochrome black T dye, EBT-Fe_2O_3 NPs complex were determined at the B3LYP 6- 311G(d,2p). The results show that the adsorption of EBT molecules caused a considerable shift in HOMO and LUMO energies. This impact might be attributable to the chemisorption type of adsorption [50]. Besides, we noticed an increase in the energy gap from (1.3483) (α-Fe_2O_3 NPs) to (0.3964 ev) (EBT-Fe_2O_3 complex), suggesting that the formed EBT-Fe_2O_3 NPs complex is less stable than isolated α-Fe_2O_3 NPs.

Table 3: The values of HOMO, LUMO, and the energy gap of EBT, α-Fe_2O_3 NPs, and EBT- Fe_2O_3 NPs complex

System	EHOMO	ELUMO	ΔE
Eriochrome black T	-5.8663	-4.1028	1.7634
α-Fe_2O_3 NPs	-5.6399	-4.2916	1.3483
EBT -Fe_2O_3 NPs	-3.2954	-2.8990	0.3964

3.3.1. Electronic density distribution

The equitable distribution of electrical charges on the optimal geometry of both adsorbent and adsorbate molecules was computed to determine the nucleophilic & electrophilic attack locations. Figure 12 shows the MEP (molecular electrostatic potential) of (EBT-Fe_2O_3 NPs). The results show that the oxygenated groups of Eriochrome black have a large a negative number charge density and are displaced on these functional areas (red color).

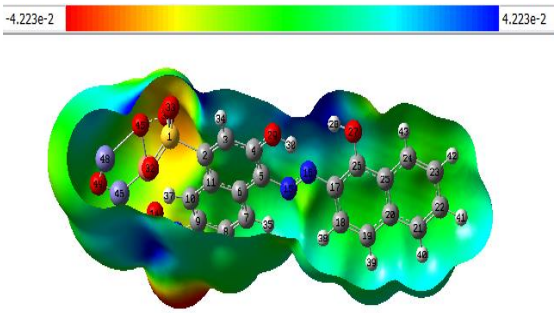

Figure 12: Distribution of the electron density on the optimized molecular geometries of the EBT - Fe_2O_3 NPs and Eriochrome black.

3.3.2. Adsorption study

We may forecast the adsorption type by comparing ΔE interaction values for a hypothesized connection between the surface and the EBT dye. Optimization operations were done using the DFT approach for the surface (EBT-Fe_2O_3 NPs). In the first state, we regard the covalent link in AEBT- Nano to be a chemical bonding, whereas the remaining states are considered interactions (physical), as illustrated in Fig. 2. According to TED and ESP calculations, the oxygen atom has a high electron density and hence serves as the active location for these interactions. The large ΔE found in this work confirms that the adsorption occurs chemically on the nanostructure surfaces.

$$\Delta \text{ Ephy or chem} = E(\text{EBT-Nano}) - (E(\alpha\text{-}Fe_2O_3 \text{ NPs}) + E(\text{EBT}))$$

E EBT-Nano is the energy of the entire system containing the EBT-Fe_2O_3 NPs

E (α-Fe_2O_3 NPs) E(EBT) represents the total energy of the surface only and the Dye only, respectively.

In chemisorption, the ΔE equal to 75.995H, whereas, in physisorption is equal to 28.077H (Table 4)

Table 4: Adsorption parameters calculated by the DFT method

Adsorption type	E(α-Fe_2O_3 NPs)[a]	E(EBT-Fe_2O_3 NPs)[a]	E(EBT)[a]	ΔE[a]
Physisorption	-2752.9	-4557.6	-1858.5	53.8129
Chemisorption	-2752.9	-4709.7	-1858.5	98.279

Fe2O3-BET

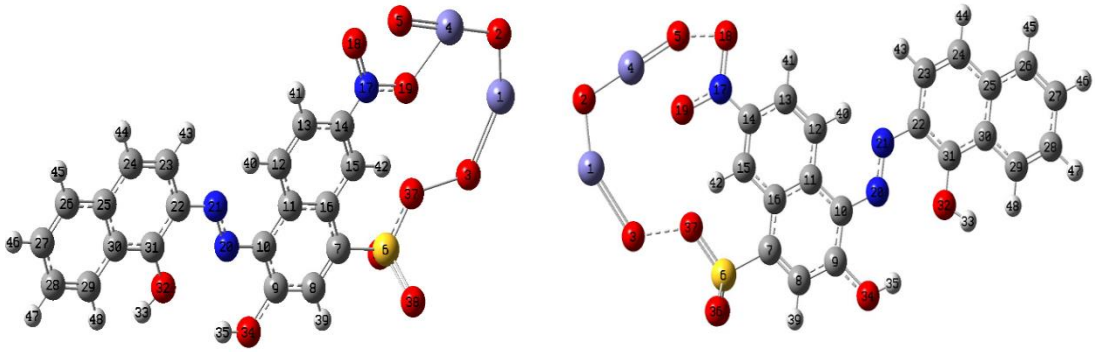

Figure 13: The interaction between the Dye and the surface of adsorbent

Conclusions

This work investigates the adsorption properties of α-Fe_2O_3 NPs for Eriochrome black t from polluted water. The α-Fe_2O_3 NPs was synthesized by the green method, and it was characterized using XRD, EDX, and SEM. Experimental dye adsorption parameters such as contact time, material dosage, and temperature had a positive effect on the adsorption of Eriochrome Black T, and the PH solution exhibited increased EBT removal in the basic medium. The results show that the Freundlich isotherms is well describing the adsorption isotherms. The overall exothermic spontaneous nature of the adsorption on Eriochrome Black T onto α-Fe_2O_3 NPs is confirmed by a negative value of Δ H, and Δ G. the pseudo-first-order model best described the kinetic uptake characteristics. The DFT study reveals significant insights into the interaction between Eriochrome black T dye (EBT) and α-Fe_2O_3 NPs. The adsorption of EBT on α-Fe_2O_3 NPs leads to a notable decrease in the

energy gap, indicating reduced stability of the EBT-Fe_2O_3 NPs complex compared to isolated α-Fe_2O_3 NPs. Furthermore, the large interaction energy in chemisorption confirms strong chemical bonding, highlighting the active role of oxygen atoms in the adsorption process.

References

[1] V. Parlak, "Classification of Pollution and Their Entry Rotues into Aquatic Ecosystems," in *Aquatic Toxicology in Freshwater: The Multiple Biomarker Approach*, 2024, pp. 123-137.

[2] K. D. Patil, "Environmental Effects and Threats of Waste: Understanding Threats and Challenges to Ecosystem, Health, and Sustainability and Mitigation Strategies," in *From Waste to Wealth*, 2024, pp. 37-69.

[3] S. Yesmin, "Piper chaba stem extract facilitated the synthesis of iron oxide nanoparticles as an adsorbent to remove congo red dye," *ACS omega,* vol. 9, no. 9, pp. 10727-10737, 2024.

[4] K. Sharma, "Water pollution: Primary sources and associated human health hazards with special emphasis on rural areas," in *Water Resources Management for Rural Development*, 2024, pp. 3-14.

[5] P. Das, "Recent advances in magnetic fluid hyperthermia for cancer therapy," *Colloids and Surfaces B: Biointerfaces,* vol. 147, pp. 42-55, 2019.

[6] K. Behl, "Cyanobacteria: a precious bioresource for bioremediation," in *Cyanobacteria*, 2024, pp. 341-382.

[7] A. Zaman, "Removal of Toxic Emerging Pollutants Using Membrane Technologies," in *Membranes for Water Treatment and Remediation*, 2023, pp. 168-208.

[8] A. Kumar, "Structure and properties of dyes and pigments," in *Dyes and Pigments: Novel Applications and Waste Treatment*, vol. 131, 2021.

[9] S. Benkhaya, "A review on classifications, recent synthesis and applications of textile dyes," *Inorganic Chemistry Communications,* vol. 115, p. 107891, 2020.

[10] A. S. Gomes, "Cationic dialdehyde cellulose microfibers for efficient removal of eriochrome black T from aqueous solution," *Bioresource Technology,* vol. 380, p. 129096, 2023.

[11] S. Kotnala, "Fabrication of nano-biocomposite for the removal of Eriochrome Black T and malachite green from aqueous solution: isotherm and kinetic studies," *Environmental Science and Pollution Research,* vol. 30, no. 10, pp. 27846-27862, 2023.

[12] M. Honarmand, "Synthesis and characterization of SnO2 NPs for photodegradation of eriochrome black-T using response surface methodology," *Environmental Science and Pollution Research,* vol.

28, no. 6, pp. 7123-7133, 2021.

[13] I. De, "In-vitro toxicity assessment of a textile dye Eriochrome Black T and its nano-photocatalytic degradation through an innovative approach using Mf-NGr-CNTs-SnO2 heterostructures," *Ecotoxicology and Environmental Safety*, vol. 243, p. 113985, 2022.

[14] El-Khawaga, Ahmed M, "A review on modern characterization techniques for analysis of nanomaterials and biomaterials," *ES Energy & Environment*, vol. 23, p. 1078, 2024.

[15] F. Mohammed, "Synthesis and Characterization of Graphene Oxide for Efficient Adsorptive Removal of Hymexazol Pesticide from Aqueous Solutions: Thermodynamic, Kinetic, and Isotherm Studies," *Al-Mustansiriyah Journal of Science*, vol. 25, no. 2, pp. 70-82, 2024.

[16] O. Gohar, "Nanomaterials for advanced energy applications: Recent advancements and future trends," *Materials & Design*, vol. 241, p. 112930, 2024.

[17] F. Mohammed, "Effective removal of Hymexazol pesticide from polluted water using cadmium oxide nanoparticles prepared by photolysis methods: Thermodynamic, kinetic, and isothermal studies," *Journal of Wildlife and Biodiversity*, vol. 7, no. Special Issue, pp. 586-600, 2023.

[18] S. Deepthi, "Comparison of cytotoxic and photoluminescence properties between Fe2O3 and Fe3O4," *Inorganic Chemistry Communications*, vol. 156, p. 111101, 2023.

[19] M.-N. Savari, Theranostic Iron-Oxide Based Nanoplatforms in Oncology: Synthesis, Metabolism, and Toxicity for Simultaneous Imaging and Therapy, 2023.

[20] S. Vihodceva, "Antibacterial activity of positively and negatively charged hematite (α-Fe2O3) nanoparticles to Escherichia coli, Staphylococcus aureus and Vibrio fischeri," *Nanomaterials*, vol. 11, no. 3, p. 652, 2021.

[21] M. Tahir, "Investigation of optical, electrical and magnetic properties of hematite α-Fe2O3 nanoparticles via sol-gel and co-precipitation method," *Journal of King Saud University-Science*, vol. 35, no. 5, p. 102695, 2023.

[22] A. Fouda, "Catalytic degradation of wastewater from the textile and tannery industries by green synthesized hematite (α-Fe2O3) and magnesium oxide (MgO) nanoparticles," *Current Research in Biotechnology*, vol. 3, pp. 29-41, 2021.

[23] R. Periakaruppan, "Phyto-synthesis and characterization of parthenium-mediated iron oxide

nanoparticles and an evaluation of their antifungal and antioxidant activities and effect on seed germination," *JOM,* vol. 75, no. 12, pp. 5235-5242, 2023.

[24] V. A. Chowdhary, "Biomolecules regulating defense mechanism in plants," *Proceedings of the National Academy of Sciences, India Section B: Biological Sciences,* vol. 93, no. 1, pp. 17-25, 2023.

[25] H. M. Esfanddarani, "Phytosynthesis of transition (Ni, Fe, Co, Cr, and Mn) metals and their oxide nanoparticles for biomedical applications: a review," *Journal of Materials Science,* pp. 1-17, 2024.

[26] P. Chen, "Selective removal of heavy metals by Zr-based MOFs in wastewater: New acid and amino functionalization strategy," *Journal of Environmental Sciences,* pp. 268-280, 2023.

[27] R. o. d. a. d. f. a. s. b. g. o. A. s. a. c. methods, "Removal of drug and dye from aqueous solutions by graphene oxide: Adsorption studies and chemometrics methods," *NPJ Clean Water,* vol. 5, no. 1, p. 5, 2022.

[28] P. Kushwaha, "Influence of different surfactants on morphological, structural, optical, and magnetic properties of α-Fe2O3 nanoparticles synthesized via co-precipitation method," *Applied Physics A,* vol. 128, no. 1, p. 18, 2022.

[29] E. Paulson, "Significance of thermal interfacing in hematite (α-Fe2O3) nanoparticles synthesized by sol-gel method and its characteristics properties," *Surfaces and Interfaces,* vol. 26, p. 101432, 2021.

[30] Y. E. Hassen, "Dodonaea angustifolia Extract-Assisted Green Synthesis of the Cu2O/Al2O3 Nanocomposite for Adsorption of Cd(II) from Water," *ACS Omega,* vol. 8, no. 19, pp. 17209-17219, 2023.

[31] F. Le Guern, "Fluorescein derivatives as fluorescent probes for pH monitoring along recent biological applications," *International journal of molecular sciences,* vol. 21, no. 23, p. 9217, 2020.

[32] M. Bansal, "Adsorption of Eriochrome Black-T (EBT) using tea waste as a low cost adsorbent by batch studies: A green approach for dye effluent treatments," *Current Research in Green and Sustainable Chemistry,* vol. 3, p. 100036, 2020.

[33] O. Marzoughi, "Adsorption of sulfur on Lanxess Lewatit® AF 5 resin during the acidic albion leaching process for chalcopyrite," *Heliyon,* p. e13112, 2023.

[34] X. Qi, "Recent advances in polysaccharide-based adsorbents for wastewater treatment," *Journal of Cleaner Production,* p. 128221, 2021.

[35] T. A. Aragaw, "A comparative study of acidic, basic, and reactive dyes adsorption from aqueous solution onto kaolin adsorbent: Effect of operating parameters, isotherms, kinetics, and thermodynamics," *Emerging Contaminants*, pp. 59-74, 2022.

[36] E. Allahkarami, "Assessment of chromite ore wastes for methylene blue adsorption: Isotherm, kinetic, thermodynamic studies, ANN, and statistical physics modeling," *Chemosphere*, vol. 358, p. 142098, 2014.

[37] O. A. Alnasra, "Enhanced removal of Pb (II), Zn (II) and Cd (II) ions by insolubilized humic acid: Characterization and sorption behaviors," *Desalination and Water Treatment*, p. 100604, 2024.

[38] É. C. Lima, "Kinetic and equilibrium models of adsorption," *Carbon nanomaterials as adsorbents for environmental and biological applications*, pp. 33-68, 2015.

[39] Z. R. Zair, "Optimization, equilibrium, kinetics and thermodynamic study of congo red dye adsorption from aqueous solutions using iraqi porcelanite rocks," *Heat and Mass Transfer*, vol. 58, no. 8, pp. 1393-1410, 2022.

[40] N. Ahadi, "Facile synthesis of hierarchically structured MIL-53 (Al) with superior properties using an environmentally-friendly ultrasonic method for separating lead ions from aqueous solutions," *Scientific Reports*, pp. 1-17, 2022.

[41] H. S. Alhares, "Sunflower Husks Coated with Copper Oxide Nanoparticles for Reactive Blue 49 and Reactive Red 195 Removals: Adsorption Mechanisms, Thermodynamic, Kinetic, and Isotherm Studies," *Water, Air, & Soil Pollution*, vol. 1, no. 35, p. 234, 2023.

[42] A. k. a. i. m. o. h. m. b. v. a. A. overview, "Wang, Jianlong," *Critical Reviews in Environmental Science and Technology*, vol. 53, no. 21, pp. 1837-1865, 2023.

[43] M. M. S. Sanad, "Graphene-magnetite functionalized diatomite for efficient removal of organochlorine pesticides from aquatic environment," *Journal of Environmental Management*, vol. 330, p. 117145, 2023.

[44] I. P. Omoregie, "Crustacean Nanochitosan-Based Bioremediation of Nanoplastic-Polluted Aquatic Habitat: A Review Pursuant to SDG 6," *Scientific African*, p. e01881, 2023.

[45] M. A. Al-Ghouti, "Guidelines for the use and interpretation of adsorption isotherm models: A review," *Journal of hazardous materials*, p. 122383, 2020.

[46] H. Patel, "Comparison of batch and fixed bed column adsorption: a critical review," *International Journal of Environmental Science and Technology*, pp. 10409-10426, 2022.

[47] Y. Zhao, "Cd (II) and Zn (II) adsorption on lignite-derived humic substances and cattle manure biochar," *CLEAN–Soil, Air, Water*, p. 2400228, 2024.

[48] M. A. Mohammad Alwi, "Two-dimensional infrared correlation spectroscopy, conductor-like screening model for real solvents, and density functional theory study on the adsorption mechanism of polyvinylpolypyrrolidone for effective phenol removal in an aqueous medium," *ACS omega*, vol. 6, no. 39, pp. 25179-25192, 2021.

[49] A. K. Maniyar, "Investigation on the Influence of Solvents Environment on the Optoelectronic Properties of the Fluorescent Probe 1, 3, 4-Oxadiazole Analogues: A Combined Theoretical and Experimental Study," *Journal of Fluorescence*, pp. 1-12, 2024.